minerals

MDPI

Article

Investigation of the Effect of Electrolytes on the Breakaway of Air Bubbles at an Underwater Capillary Using High-Speed Cinematography and Passive Acoustic Techniques

Pengbo Chu [1,*], Ronghao Li [2], Mark Lepage [2] and Kristian Waters [2]

[1] Department of Mining and Metallurgical Engineering, University of Nevada, Reno, 1664 North Virginia St., Reno, NV 89557, USA
[2] Department of Mining and Materials Engineering, McGill University, 3610 Rue University, Montreal, QC H3A 0C5, Canada; ronghao.li@mail.mcgill.ca (R.L.); mark.lepage@mail.mcgill.ca (M.L.); kristian.waters@mcgill.ca (K.W.)
* Correspondence: pengboc@unr.edu

Abstract: Saline water froth flotation has received increasing attention in recent years due to sustainability-related concerns. Although the presence of electrolytes in these flotation systems is known to produce the desired bubble swarms, i.e., a macroscopic observation, the fundamental mechanism through which the solutes produce such an effect at the microscopic level remains obscure. For example, there is no agreed mechanism (i.e., break-up or coalescence—two major bubble formation mechanisms) of how the effect is achieved. Not only is understanding the impact of electrolytes on the bubble formation mechanisms a fundamental question, but it can also provide insight into the design of more efficient air dispersing mechanisms for saline flotation systems. Previous studies have demonstrated that electrolytes can inhibit coalescence, but their potential impact on break-up remains vague, which is the focus of this study. It is hypothesized that electrolytes have an impact on break-up, and by isolating break-up from coalescence, the effects of electrolytes on break-up can be revealed. A break-up-only bubble formation system was built. Under this condition, any impact from the electrolytes on the produced bubble can be attributed to an impact on break-up. High-speed cinematography and a passive acoustic technique were employed to capture the bubble size, acoustic frequency, and damping ratio during the break-up process. Under the quasi-static condition, an increase in the electrolyte concentration increased the bubble size produced via break-up, contradicting the common observations made for bubble swarms. The break-up imparted an initial capillary wave to the bubble surface, which is correlated with the bending modulus of the air/water interface affected by the electrolytes. No direct correlation was observed between the acoustic damping ratio and that of the capillary wave, suggesting that the electrolytes affect the break-up via a different mechanism from that by surfactants.

Keywords: froth flotation bubbles; break-up; electrolytes; acoustic frequency; acoustic damping ratio; capillary wave

check for updates

Citation: Chu, P.; Li, R.; Lepage, M.; Waters, K. Investigation of the Effect of Electrolytes on the Breakaway of Air Bubbles at an Underwater Capillary Using High-Speed Cinematography and Passive Acoustic Techniques. *Minerals* **2022**, *12*, 972. https://doi.org/10.3390/min12080972

Academic Editor: Saeed Chehreh Chelgani

Received: 19 July 2022
Accepted: 28 July 2022
Published: 30 July 2022

Publisher's Note: MDPI stays neutral with regard to jurisdictional claims in published maps and institutional affiliations.

Copyright: © 2022 by the authors. Licensee MDPI, Basel, Switzerland. This article is an open access article distributed under the terms and conditions of the Creative Commons Attribution (CC BY) license (https://creativecommons.org/licenses/by/4.0/).

1. Introduction

Bubble formation in the presence of electrolytes has been found in many natural and engineering processes. Bubbles formed at the sea surface determine how air is mixed into the ocean and water is mixed into the atmosphere—two processes that have a significant impact on climate [1]. In gas–liquid reactors, bubbles also play a critical role as their size determines the available interfacial area, thereby affecting the heat and mass transfer [2,3]. One process where bubbles are of great significance is froth flotation. In this process, air bubbles act as vehicles to selectively collect and transport valuable mineral particles from a mixed-particle suspension. To ensure the process efficiency, the bubbles must be small to provide larger interfacial area but, at the same time, have sufficient buoyancy to float

the collected mineral particles [4–7]. A typical bubble size required ranges from 0.5 to 2.5 mm, but such bubble sizes are difficult to achieve in pure water because the lack of solutes cannot prevent coalescence [8–10]. As a result, frothers (a class of surfactants) are commonly utilized to assist the production of small bubbles. In addition to frothers, some inorganic salts (electrolytes) are also known to be capable of producing a similar effect.

The role of frothers and salts on small-bubble production has been generally ascribed to their ability to hinder coalescence [11–16]. A commonly accepted mechanism is that the presence of these solutes changes the intermolecular forces and surface rheology of liquid films between approaching bubbles [15]. Sufficient understanding of this mechanism has been achieved for the case of frothers [14,17]. However, questions still remain to be answered for salts [18]. Of the existing literature, there are a few studies regarding salts. For example, in the work of Craig et al. (1993), the authors studied a wide range of cations and anions on bubble coalescence in water [14]. They found that different combinations of cations and anions affect the behavior of the salts tested. They speculated that the specific effects of electrolytes on bubble coalescence may be related to their effect on water structure and, thus, the hydrophobic interaction. In another study by Hofmeier et al. (1995), the bubble coalescence was investigated against the surface elasticity impacted by sodium chloride [2]. It was found that in solution where the surface elasticity is large, bubble coalescence is inhibited. The surface tension gradient was another parameter that had been investigated. In the study completed by Weissenborn et al. (1996), the researchers correlated the surface tension/electrolyte concentration gradients to the mechanism of coalescence inhibition [16]. They found that the Gibbs–Marangoni effect caused by the surface tension gradients did not provide a satisfactory explanation for the coalescence prevention. Aside from the chemistry aspect, the physical condition also has an indisputable role. In a recent investigation by Filippov et al. (2018), the role of chloride salts on bubble coalescence was studied [19]. They found that the coalescence prevention is affected not only by the concentration of salts but also the ion–water, ion–ion, and water–water properties as a function of hydrodynamic condition.

While the bulk of the literature emphasizes the role of salts in coalescence inhibition, an important aspect being omitted is whether salts have any impact on break-up. In fact, there are occasional references suggesting that the presence of salts indeed has an impact on break-up. A relevant work is by Kracht and Finch (2009), where the authors investigated the role of sodium chloride on the break-up of a mono-size distribution of bubbles subjected to a turbulent field. They found that the presence of NaCl not only decreases the coalescence but also promotes the break-up. However, a notable drawback of their technique is that break-up and coalescence take place simultaneously, which makes it difficult to distinguish the type of mechanism that affected the salt. To overcome this deficiency, Chu et al. (2016) developed a new experimental setup that was able to isolate break-up from coalescence so that the effect of frothers and salts on the break-up in turbulent conditions can be accurately assessed [20–22]. Their observation was that the presence of solutes generally affects the break-up by producing smaller bubble sizes until a certain concentration is reached, after which the trend becomes adverse. To further explore the break-up phenomena, another study was carried out by the same group where air bubbles were slowly generated at a capillary tube in froth solutions under a quasi-static condition [4]. The experiment was monitored using high-speed cinematography and passive acoustic techniques allowing microscopic features associated with break-up to be revealed. The study found that frothers indeed affect the break-up by generating smaller bubble sizes, and that the microscopic features, i.e., capillary wave fluctuations observed from the imaging and the acoustic damping ratio observed from the acoustic technique, are correlated. They attributed the surface tension gradients imparted by the frother molecules as responsible for these actions.

The objective of this work is to employ the experimental techniques developed by Chu et al. (2017) [4] to study the role of salts on the breakaway of underwater air bubbles at a capillary. As the high-speed cinematography and passive acoustic techniques provide a real-time and continuous measurement, it is expected that new insights associated with

the break-up in the presence of salts will be revealed. The study is compared with that of the frothers to identify any mechanism that arises due to the presence of salts.

2. Materials and Methods

The experimental setup is shown in Figure 1. The plexiglass tank has a dimension of 21.5 cm (L) × 21.5 cm (W) × 16 cm (H), holding 2.5 L of solution in which air bubbles are produced via a glass capillary with an internal diameter of 4 mm. The air flow rate was regulated using a needle valve. The bubble breakaway from the capillary was monitored using a Fastec high-speed camera (HiSpec5 8G Mono) equipped with a 60 mm macro lens (Nikon, AF Micro). The passive acoustic signal emissions were monitored using a hydrophone (Lab-40 hydrophone from LABcore System) shown in Figure 1 with a detectable frequency range of 5−85000 Hz. Acquisition of the acoustic signal was obtained using a National Instrument data acquisition system (NI USB-6341, X Series DAQ) at a rate of 500 kHz to minimize aliasing issues. The complete setup was placed on a supercushioning foam slab (McMaster Carr, 3/4 in. thick blue polyurethane, 86195K35) to minimize extraneous vibrations that could corrupt the bubble breakaway process.

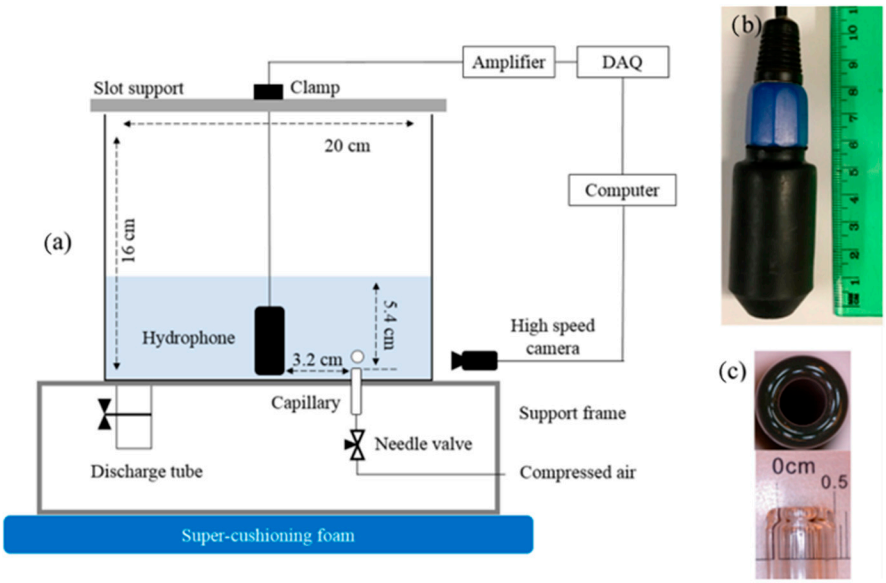


Figure 1. Experimental setup, adapted from Chu et al. (2017) [4]. Copyright 2017 ACS Publications. (**a**) overview of the entire setup, (**b**) hydrophone, and (**c**) capillary.

Five salts were tested, and their solutions were prepared in reverse osmosis (RO) water at room temperature of approximately 23 °C. Table 1 shows the molecular weight, purity, and manufacturer of the salts tested.

Table 1. Salt tested.

Salts	M.W. (g/mol)	Tested range (M)	Purity	Manufacture
NaCl	58.44	0–0.35	99.8%	Fisher Scientific
KCl	74.55	0–0.35	≥99.0%	Fisher Scientific
Na_2SO_4	142.04	0–0.35	≥99.0%	Sigma-Aldrich
$CaCl_2 \bullet 2H_2O$	147.01	0–0.35	≥99.0%	Sigma-Aldrich
$MgCl_2 \bullet 6H_2O$	203.30	0–0.35	≥99.0%	Sigma-Aldrich

The position of the hydrophone critically affects the quality of the acoustic signal as a result of the bubble breakaway event. The hydrophone itself could be a disturbance if located near the acoustic source; conversely, if it is too far away, the acoustic signal would be too weak and shielded by background noise. The position of the hydrophone was

determined by trial and error, and it is shown in Figure 1a. To minimize the interference made other than the presence of salts, a quasi-static condition was maintained for all the experiments. To achieve this condition, a needle valve with a fixed opening was utilized to minimize the flow turbulence. All salt solutions were prepared by adding the desired amount of salt into 2.5 L of Reverse Osmosis (RO) water, and then mixing with a magnetic stirrer to ensure a uniform concentration. The experiments started with highspeed image recording, during which at least four bubble breakaways were captured. Next was the acoustic signal recording, where each measurement included at least four bubble breakaway acoustic emissions. After an experiment was completed, the tank was emptied and rinsed with RO water. Each test condition was repeated at least three times to obtain the mean and 95% confidence interval (CI). Following the experiment, the recorded images were analyzed to obtain the bubble size and aspect ratio, and acoustic signals for frequency and damping ratio. These analysis techniques are presented in the Appendix A.

3. Results

3.1. Observations from Highspeed Cinematography

An example of a bubble breakaway in RO water is shown in Figure 2. The sequence shows that the breakaway generates two major phenomena. One is the rapid formation of a liquid jet immediately following the break of the thin air neck. The other is the formation of a surface wave, i.e., a capillary wave, as a result of the rapid dissipation of the liquid jet. This surface wave perturbates to the bubble surface, which travels upward along the bubble surface. The image sequence also shows that the surface wave travels at an exceeding velocity compared to the rising velocity of the air bubble, i.e., the air bubble barely moves within the time frame captured in Figure 2.

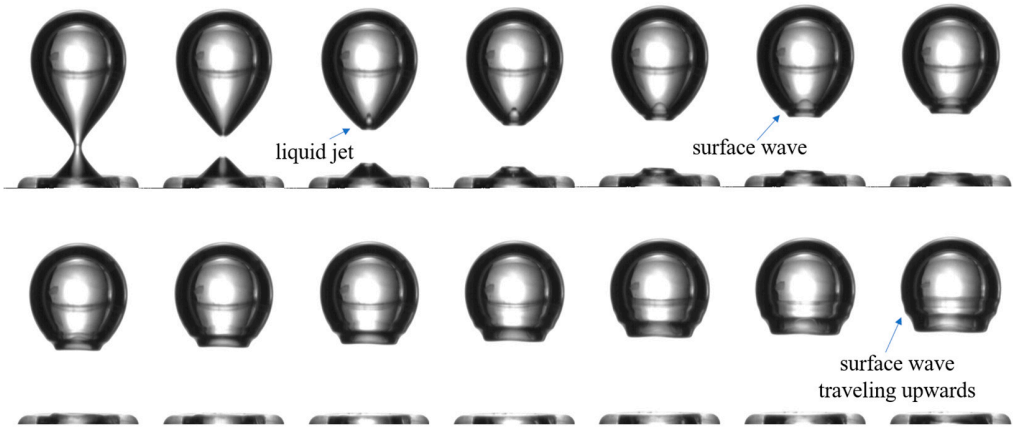


Figure 2. A bubble breakaway event in RO water and subsequent surface wave; images were continuously taken at 6000 frames per second.

The formation of the liquid jet and surface wave was observed in all salt solutions tested. While it was challenging to observe the variation in the resulting surface wave propagation, the imaging sequence revealed that the maximum height of the liquid jet was affected by the presence of the salts. Figure 3 shows an example of the maximum height of the liquid jet in NaCl solutions (the other salts shown in Appendix A). The height was measured from the second image immediately after the breakaway (for instance, the third image in Figure 2 for RO water) and was normalized to that in the RO water. The results indicate that among the salts tested, sodium chloride and sodium sulfate seem to produce a similar effect. It appears that both salts tend to increase the maximum jet height at their low salt concentrations, ca., NaCl at 0.025 M increases the maximum jet height to 114% $\pm$ 14% (95% C.I.) of that in the RO water; Na_2SO_4 at 0.025 M to 128% $\pm$ 4%. A further increase in the salt concentration causes the maximum height of the jet to decrease. For potassium chloride and calcium chloride, the general observation is that increasing the salt concentration decreases the maximum jet height, with potassium chloride producing

a larger reducing effect. The presence of magnesium chloride does not seem to affect the maximum jet height.

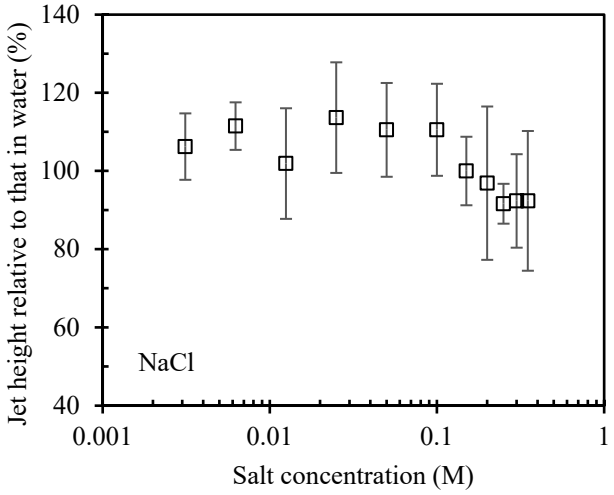


Figure 3. Maximum jet height in different salt solutions.

The liquid jet dissipates, forming a surface wave that acts as an initial perturbation to the bubble surface. One consequence of this surface wave is that it affects the magnitude of the bubble surface oscillation, which can be observed from the bubble shape characterized by the aspect ratio. Figure 4a illustrates an example of the change in aspect ratio influenced by the hydrodynamics in RO water. The results show that the bubble shape first tends to become spherical, i.e., the aspect ratio reduces to 1, at, ca., 3 milliseconds after the breakaway. The oscillation then continues, which causes a larger distortion to the bubble shape. The image on the top right of Figure 4a shows a severely distorted bubble in RO water at, ca., 11 milliseconds after the breakaway.

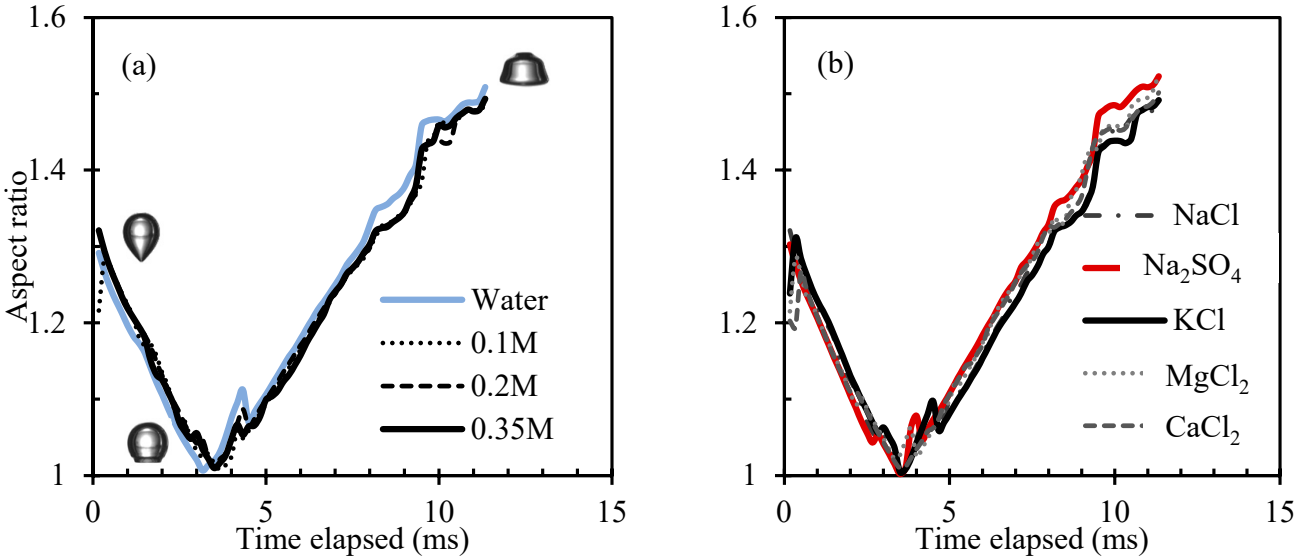


Figure 4. Aspect ratio: (**a**) in water and NaCl solutions (bubble images taken in RO water); (**b**) in 0.35 M salt solutions.

The bubble shape is not only affected by the hydrodynamics but also likely by the presence of salts. Figure 4a also shows the effects of NaCl concentration on the aspect ratio. As observed, the aspect ratio in NaCl solutions exhibits a similar trend to that in the RO water. However, it seemed to be affected by the presence of NaCl, especially later when the bubble rises further up. A relatively notable observation is at ca. 5 milliseconds (and onwards) when the increasing NaCl concentration seems to start to suppress the aspect ratio, i.e., the aspect ratio tends to become closer to 1. This observation can also be found in other salt solutions tested (results provided in Appendix A). However, it should be noted that the current observation was made through visual inspection. Future studies will be required to confirm any statistical difference among these observations.

In understanding the impact of the salt type on the aspect ratio, this investigation has found that the potassium chloride and sodium sulfate, in general, produce the most prominent effect. Figure 4b shows the aspect ratio in 0.35 M salt solutions. The observation is that the maximum or minimum aspect ratio is almost always a result of either KCl or Na_2SO_4. During the first oscillation cycle, i.e., right after the breakaway but prior to aspect ratio 1 at, ca., 3.5 ms, the maximum aspect ratio is dominated by KCl, whereas the minimum is dominated by Na_2SO_4. As the oscillation continues, the trend reverses, and the difference becomes more profound as more time elapses.

3.2. Acoustic Analysis

The acoustic analysis generated two types of results: the acoustic frequency and damping ratio.

An example of the acoustic frequency in NaCl solutions is shown in Figure 5a. The figure also includes the bubble size calculated using the Minnaert relationship and that estimated from the image analysis. It is obvious that the increasing salt concentration reduces the acoustic frequency; however, the reduction is typically small. The other salts tested show a similar effect, though the degree of reduction may vary. The acoustic frequency in other salt solutions can be found in the Appendix A.

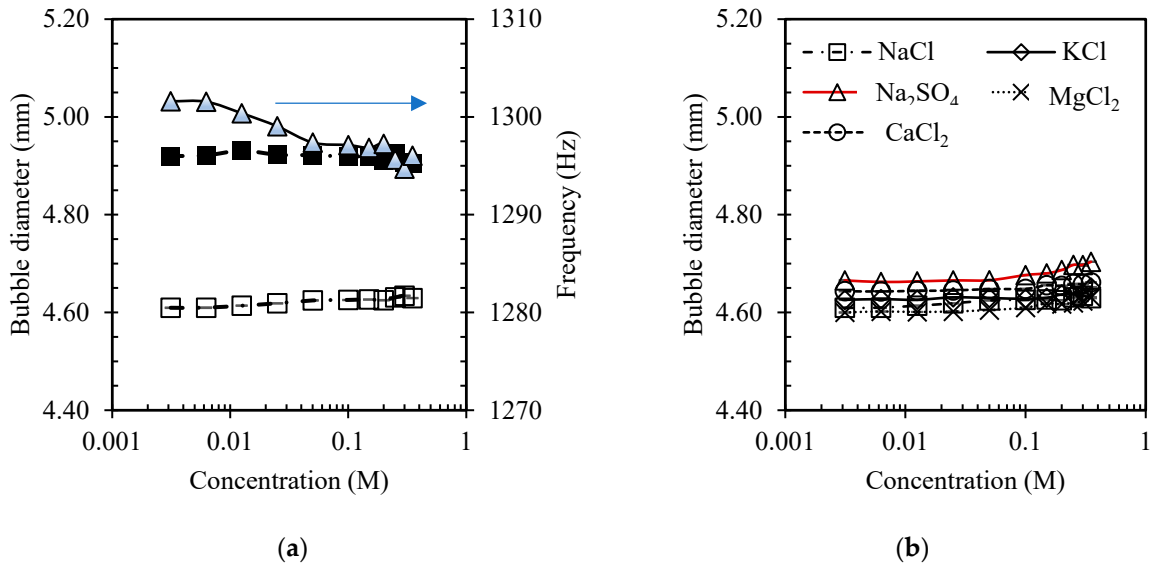


Figure 5. Bubble size in salt solutions: (**a**) Acoustic frequency vs. bubble size. The solid triangles with a gradient represent the acoustic frequency; the black squares are the bubble size estimated from image analysis; the open squares are the bubble size estimated from the Minnaert relationship. (**b**) Acoustically determined bubble size in different salt solutions.

As the acoustic frequency shows an inverse trend with the bubble size from the Minnaert relationship, the small reduction in the acoustic frequency means little change in the bubble size with increasing salt concentration. This is consistent with the bubble size estimated from the imaging result. As shown in Figure 5b, the presence of salts (i.e., concentration up to 0.35 M) has caused a minor increase in the bubble size with respect to that in the RO water. The change is 0.12% for NaCl, 1.73% for Na_2SO_4, 0.58% for KCl, 0.81% for $CaCl_2$, and 0.15% for $MgCl_2$.

The normalized acoustic damping ratio (i.e., with respect to RO water) as a function of the salt concentrations is shown in Figure 6, where two general observations can be made. One is that all salts show a decrease in the damping ratio as the salt concentration increases. Though calcium chloride and sodium sulfate exhibit some adverse trends at their high salt concentrations, the overall decreasing trend for both salts is still valid. The other is that the chloride salts amplify the damping ratio beyond that of the RO water at their low salt concentrations, while sodium sulfate immediately diminishes it below. For example, at 0.00313 M, the initial increase in the damping ratio is about 7% for $MgCl_2$, 5% for both $CaCl_2$ and NaCl, and 3% for KCl, while the decrease is about 6% for Na_2SO_4.

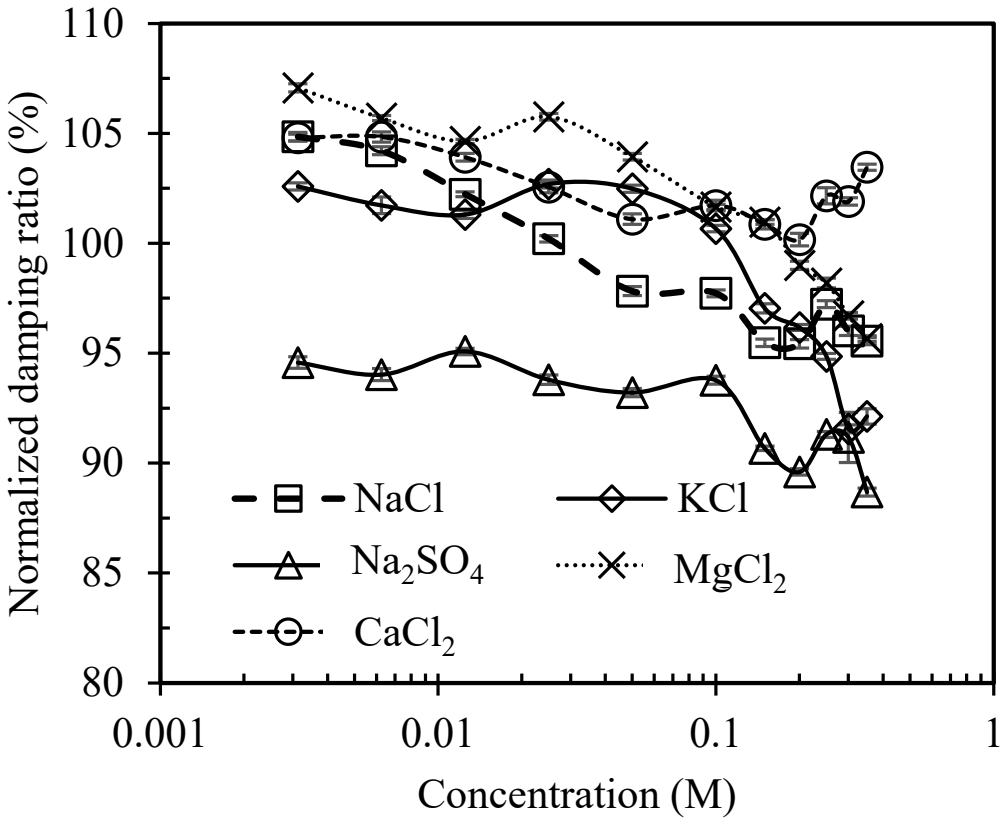


Figure 6. Normalized damping ratio (i.e., relative to that of RO water shown as red dashed line) as a function of the salt concentration.

4. Discussion

4.1. Bubble Size

The current investigation only focused on single bubble formation via the break-up mechanism and the system did not involve the use of frothers. The results show that the presence of salts increases the bubble size produced, which appears to contradict the common observation made for bubble swarm systems. To explain the phenomenon, a re-visit to the fundamental break-up mechanism is necessary. Prior to break-up, an air/water interface must be deformed. This deformation results from the hydrodynamic stress in the liquid (e.g., turbulent eddies) and surface stress (e.g., surface tension) [23,24]. These stresses affect the interface in different ways—whereas the former tends to disrupt it, the latter

attempts to restore and maintain a minimum surface area. Consequently, the competition between these actions determines the outcome of the break-up, such as the resulting bubble size [25]. In the current study, the hydrodynamic stress can be viewed as constant in all the tested solutions because a quasi-static condition has been precisely maintained. The only changing condition then can be assumed as the surface properties as a result of the presence of salts. Among different surface properties, this work focuses on the surface tension. It is well known that many salts, including most in the present study, generally increase the surface tension of water [2,16,19,26]. On this basis, it is reasonable to hypothesize that the increasing surface tension would result in a large bubble size because the interface has more strength to work against the external perturbation (i.e., hydrodynamic stress caused by the injected air) prior to its breakup. This hypothesis seems to be well supported by Figure 7a where the relative change in bubble size is plotted against that in surface tension, showing a unique linear relationship for each salt tested.

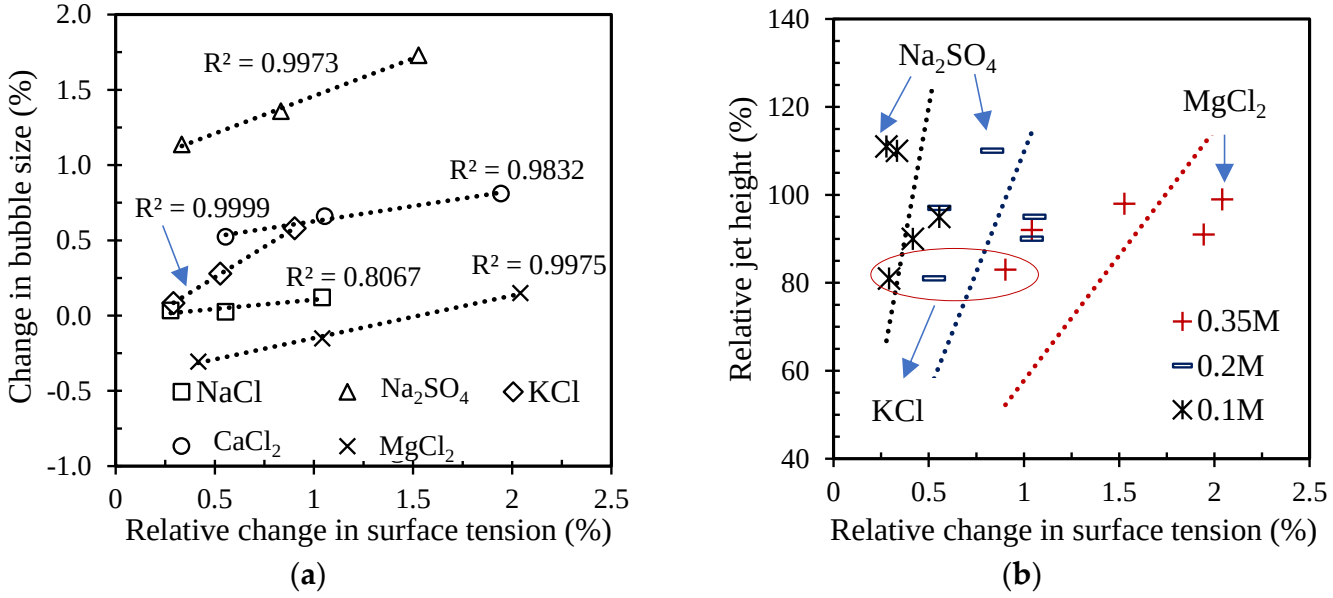


Figure 7. (**a**) Relative change in surface tension vs. change in bubble size, (**b**) relative change in surface tension vs. change in bubble size. A surface tension data range from 0.1 to 0.35 M was obtained from [16].

The analysis in Figure 7a also shows that over the tested salt concentrations (up to 0.35 M), KCl causes the smallest increase in the surface tension; however, it renders the fastest rate of change in the bubble size affected by the change in surface tension (i.e., slope 0.8117). KCl is the only structure breaking salt in this study; its presence is believed to cause disruption to the intermolecular hydrogen bonding of water molecules [26]. Therefore, a small influence on the surface tension by KCl is an expected observation. The interrupted intermolecular hydrogen bonding leads to a loose hydrogen bonding network that reduces the stability of the interface against external perturbations [19]. The consequence is that the interface turns out to be more prone to external perturbations, becoming easier to break. This might be the reason the change in bubble size is more receptive to the change in surface tension in KCl solutions.

4.2. Capillary Wave

In addition to the bubble size, the presence of salts also affects the initial capillary wave (i.e., the liquid jet) formed immediately after the breakaway. Figure 3 shows that the liquid jet height appears to be associated with the salt type and concentration. This relationship can be explained by the change in the surface tension as well. Figure 7b shows some evidence. The figure summarizes the relative jet height, which can reviewed as the magnitude of the initial capillary wave for all the salts at three concentrations, 0.1 M, 0.2 M, and 0.35 M. It can be observed that despite some inherent difference imparted by the salt type, the change in the jet height generally corresponds to the change in surface tension. For example, the higher salt concentration causing a larger increase in surface tension (i.e., red cross symbols) suppresses the growth of the initial jet height (i.e., the trendline has the smallest slope), which can be attributed to the previous argument that the higher surface tension renders more strength, slowing the distortion of the interface.

The effect of the salt type on the magnitude of the initial capillary wave is another observation in Figure 7b. It is noted that the minimum jet height is always associated with KCl, while the maximum is generally associated with Na_2SO_4 until, at higher concentration, it is taken over by $MgCl_2$. The current experiment shows that each salt solution produces a unique jet height, hinting that the capillary wave is affected by the salt type. This is consistent with the observation by Chen et al. [27]. They conducted molecular dynamics simulations to study the effect of salt ions on the bending modulus of an air/water interface and found that the bending modulus is inversely related to the magnitude of the capillary wave fluctuation. Among the studied salts including NaCl, $CaCl_2$, and $MgCl_2$, they found that $MgCl_2$ (0.5 M) produced the smallest bending modulus, implying that the presence $MgCl_2$ triggered the largest capillary wave fluctuation. This is consistent with the observation in this work that $MgCl_2$ at high concentration results in the largest jet height. With that, one can also rank the impact of the salts on the capillary wave fluctuations. For example, at the maximum concentration of 0.35 M tested in the present work, the order follows: $MgCl_2$ (relative jet height is 99 $\pm$ 7%) > Na_2SO_4 (98 $\pm$ 11%) > NaCl (92 $\pm$ 18%) > $CaCl_2$ (91 $\pm$ 6%) > KCl (83 $\pm$ 14%).

4.3. Acoustic Analysis

The analysis of the acoustic signals also generates some important observations. It has been shown in Figure 5a that the estimated bubble size using the acoustic frequency by the Minnaert relationship is consistent with that obtained from the imaging analysis. Although there is a steady offset between the acoustic and imaging trends, the acoustically estimated bubble size is assumed to be more accurate because it is directly correlated with the volume of the produced bubble [4,28].

The analysis of the acoustic damping ratio shows that each salt is accompanied with a unique trend. Figure 6 shows that among all the salt solutions, Na_2SO_4 is generally associated with the smallest acoustic damping ratio. It has been understood that the acoustic signal emitted from a bubble is due to the volumetric pulsation of the entrapped air mass, and the acoustic damping ratio describes how fast the bubble sound decays [28,29]. It is also known from classical mechanics theory that the damping ratio is inversely related to the mass of the oscillating object [30,31]. Based on this, one can postulate that a system oscillating with a large mass should be accompanied with a smaller damping ratio, which seems to be the case for the present study. As summarized previously in Figure 5b, the Na_2SO_4 solution generally produces the largest bubble size, suggesting that the mass of the air that undergoes the acoustic oscillation in Na_2SO_4 solutions is largest. Therefore, the resulting acoustic damping ratio is smallest. Figure 8 provides more evidence to further support this argument. Regardless of the type of the salt, the observation is that a larger bubble is generally associated with a smaller acoustic damping ratio.

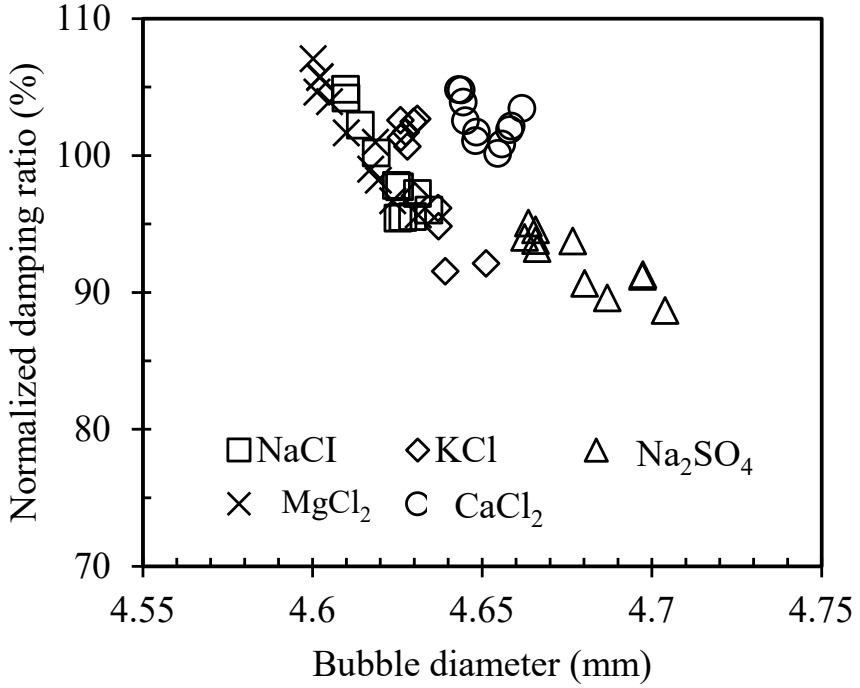


Figure 8. Normalized acoustic frequency as a function of the bubble size estimated by the Minnaert relationship.

4.4. Comparison with Previous Frother-Related Work

The acoustic damping ratio in the salt solutions does not show direct correlation with that of the capillary wave, suggesting that the salts may contribute a different mechanism from that by frothers. In a previous frother-related study, the acoustic damping ratio was shown to be inversely related to the damping of the capillary wave characterized by the aspect ratio. This was based on the assumption that the concentration of frothers was too small to cause any thermal damping, and that the total damping of the air bubble was only due to the acoustic damping and capillary wave damping [28,32]. In the present study, thermal damping cannot be ignored, because the presence of the salts can cause either exothermic or endothermic reactions, which consequently affect the surface properties. This could be why the acoustic damping ratio did not show any direct correlation with the damping of the capillary wave in the present work.

In previous studies, it was also found that larger acoustic damping ratios were generally associated with large bubbles. However, the trend was completely opposite in the current study. The difference can be attributed to the presence of surface tension gradients. In frother solutions, surface tension gradients readily exist because the dosage of the frother is typically so small (i.e., a few parts per million) that a uniform frother concentration is difficult to achieve at the air/water interface [5,33]. It is also known that the surface tension gradients can dampen the capillary wave fluctuations [34–37]. On this basis, one can anticipate that under the same frother concentration, big bubble surfaces are likely to experience less dampening because the magnitude of the surface tension gradients is small. As a result, the surface of the large bubble will be more distorted, i.e., a smaller capillary wave damping ratio, which is reflected as a large acoustic damping ratio perceived by the passive acoustic technique. For the case of salts, the concentration is much higher, so it is quite possible that a uniform ion distribution at the air/water interface can always be maintained especially under quasi-static conditions. Therefore, the presence of the surface tension gradients is unlikely. The damping ratio of the capillary wave in salt solutions is possibly controlled by other surface properties, such as the previously discussed bending modulus, which requires further investigation.

5. Conclusions

Increasing salt concentrations causing increases in the bubble size by break-up is the most striking finding from the present work because it contradicts the well-known fact that the salt solutions generally reduce bubble size [7,14,15,19,38]. In the current work, break-up of the injected air mass is the only bubble formation mechanism, whereas in the bubble swarm, break-up and coalescence co-exist and their interaction determines the bubble size. Most of the literature ascribe the role of salts on bubble size reduction to their ability to prevent coalescence as some salt ions appear to retard the drainage of inter-bubble film [2,7,14,17,39,40], which can be certainly demonstrated. There are also studies hinting at the role of the enhanced break-up, which is due to the presence of salts generating surface tension gradients promoting the breakaway of smaller bubbles [5,22,38,41,42]. The finding from this work suggests that the surface tension gradient is likely not responsible; rather, the change in surface tension resulting from the salts seems to play a significant role. The study also reveals that break-up in the presence of the salts affects the stability of the bubble surface by imparting a capillary wave of different magnitude, suggesting that the salts not only affect the produced bubble size but also the bubble stability at its birth stage. The finding offers a supplementary understanding to the existing literature that salts influence the bubble stability as it moves in gas–liquid systems [43–46]. Lastly, the study also demonstrated that the passive acoustic technique is capable of capturing microscopic information such as frequency and damping ratio of the oscillating bubble. The finding shows that the damping ratio of the acoustic signal resulting from the break-up is not correlated with that of the capillary wave on the newly formed bubble surface, implying that the mechanism through which the salts affect the interface is not the same as that resulting from surface tension gradients for the case of frothers [4,5,41]; rather, other factors such as bending modulus should also be considered [27].

In conclusion, this work provides strong experimental evidence that the presence of the salts indeed increases the bubble size produced via break-up under quasi-static conditions. Though contradicting the known effect that salts reduce the bubble size in swarms, the current system only investigated the break-up-only mechanism and the study did not involve the use of frothers. The findings suggest that the effect of salts on bubble formation seems to be manifested through their impact on coalescence prevention, and frothers are still required to achieve the desired bubble size. Nevertheless, the finding offers new insights into the understanding of transport phenomena in systems involving bubbles. To broaden the breadth of this research topic, future work should consider systems containing mixed salts, and salts with surfactants or solids. An in-depth analysis of the acoustic signals should also be performed to increase the applicability of the acoustic technique to probing phenomena at various interfaces, particularly those in opaque systems.

Author Contributions: Conceptualization, P.C. and R.L.; methodology, P.C.; software, P.C. and M.L.; validation, P.C., R.L. and M.L.; formal analysis, P.C.; investigation, R.L.; resources, K.W.; data curation, R.L. and P.C.; writing—original draft preparation, P.C.; writing—review and editing, K.W.; visualization, P.C., R.L. and M.L.; supervision, K.W.; project administration, K.W.; funding acquisition, K.W. All authors have read and agreed to the published version of the manuscript.

Funding: This research was funded by the Natural Sciences and Engineering Research Council of Canada (NSERC) Discovery Grant, grant number RGPIN05419-2019.

Data Availability Statement: Not applicable.

Acknowledgments: Chu would like to acknowledge the support of Nevada Gold Mines through their endowed professorship for this work.

Conflicts of Interest: The authors declare no conflict of interest.

Appendix A

A1. Image Processing

The equivalent bubble diameter, d_b, was determined using image analysis performed in MATLAB's Image Processing Toolbox using a custom algorithm. First, the bubble volume, V_b, was calculated by discretizing the bubble into thin volume slices, one pixel in height, along the height of the bubble and summing these thin slices. Assuming the bubbles to be cylindrically symmetrical, each thin slice represents a differential volume element, dV, which is defined by Equation (A1) and shown schematically in Figure A1.

$$dV = \frac{\pi}{4} d_{b,z}^2 \, dh \tag{A1}$$

where dh is the height of the differential volume element, in this case, constant at 1 pixel, and $d_{b,z}$ is the diameter of the bubble at some height, z, along the bubble, which is extracted using image processing.

The total volume of the bubble was then determined by summing the differential volume elements along the height of the bubble, represented by Equation (A2).

$$V_b = \sum_{z=1}^{n} \frac{\pi}{4} {d_{b,z}}^2 h \tag{A2}$$

where n is the height of the bubble in pixels. For the images analyzed, n ranged approximately between 140 and 250 pixels. With the volume of the bubble determined, the equivalent bubble diameter was then calculated by Equation (A3).

$$d_b = \sqrt[3]{\frac{6}{\pi} V_b} \tag{A3}$$

The analysis of the acoustic signals was performed using the MATLAB program developed by Chu et al. (2017), which includes three steps. In the first step, digitation at 500 kHz was applied to the raw data to ensure that microscopic features of the data were not ignored. After that, a fast Fourier transformation (FFT) was conducted to obtain the Minnaert frequency and that of the background noise. With the identified frequency of the background noises, the second step was to apply an eighth-order Butterworth bandpass filter to remove those noises. The last step was to model the filtered bubble signals in the time domain with a sinusoidal decay function shown in Equation (A4).

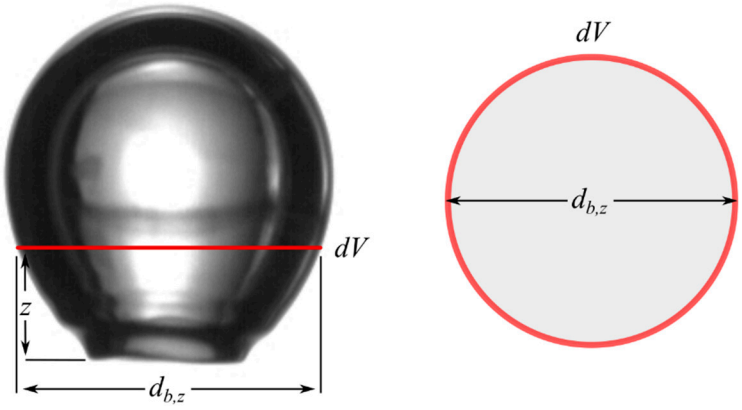


Figure A1. Schematic of the differential volume element dV in determining the bubble volume.

$$(t) = Ae^{-\zeta\omega_0 t} \cos\left(\omega_0 \left(\sqrt{1-\zeta^2}\right) t + \varphi\right) + C \tag{A4}$$

where A is the amplitude, ω_0 is the undamped frequency (Hz), ζ is the damping ratio, φ is the phase angle (in radian), and C is a constant. The acoustic frequency was used to predict the bubble size using the Minnaert relationship shown in Equation (A5).

$$f = \sqrt{3kP_0/\pi^2 d^2 \rho} \quad \text{(A5)}$$

where f is the sound frequency (Hz), d is the bubble diameter (m), k is the ratio of specific heats for the gas, P_0 is the liquid pressure (Pa), and ρ is the liquid density (kg/m^3).

A2. Jet Height in Different Salt Solutions

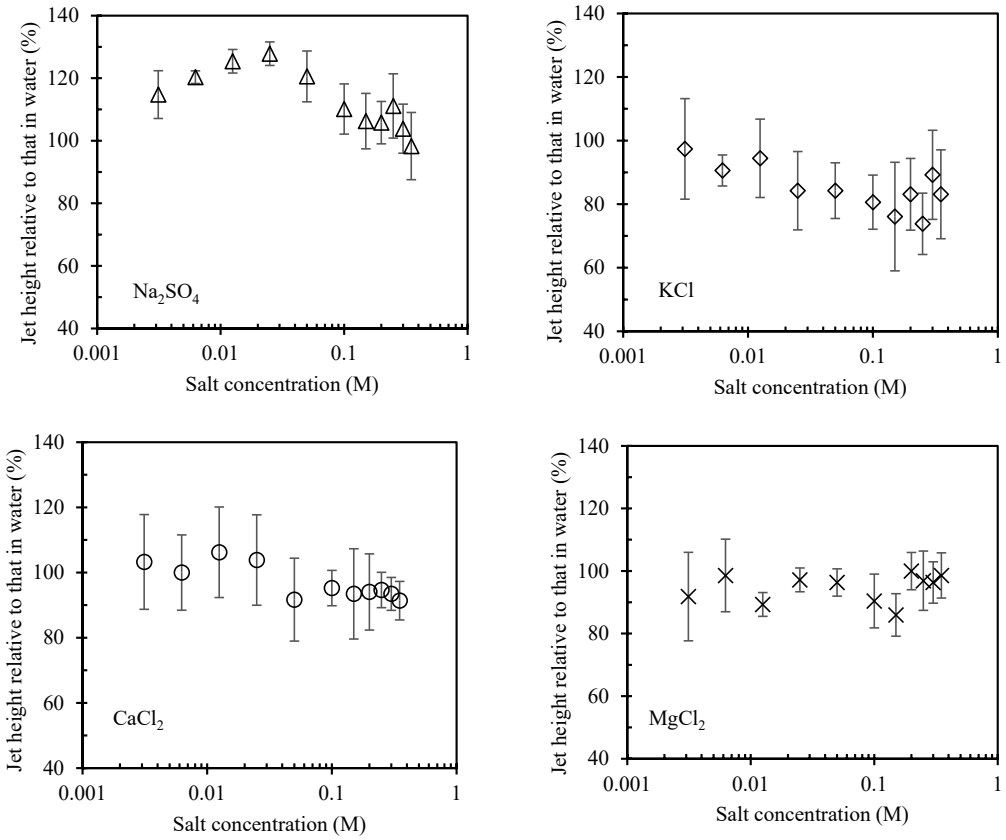


Figure A2. Maximum jet height in different salt solutions (Na_2SO_4, KCL, $CaCl_2$ and $MgCl_2$).

A3. Aspect Ratios

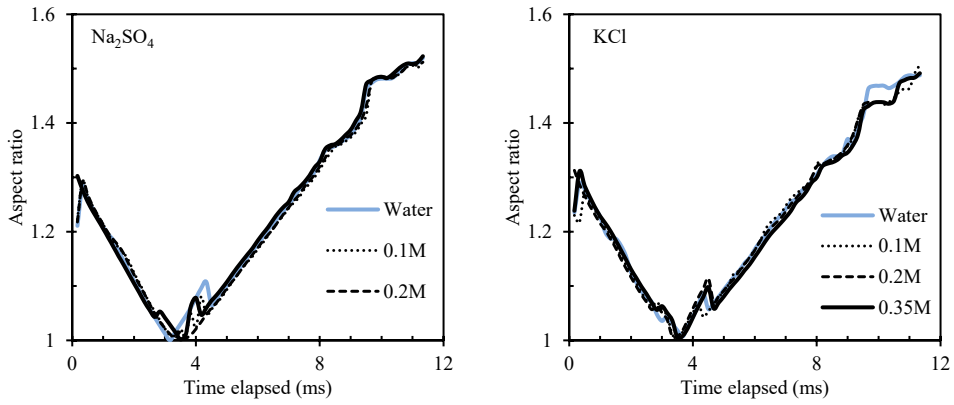


Figure A3. *Cont.*

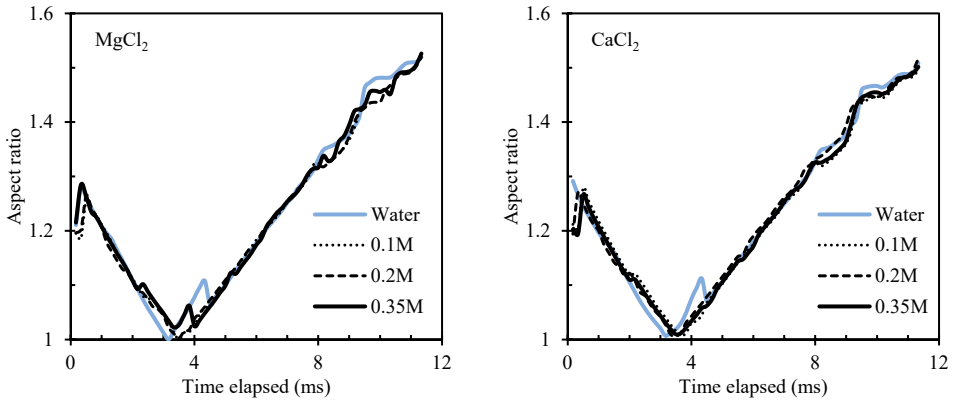


Figure A3. Aspect ratio in different salt solutions.

A4. Acoustic Damping Ratio and Frequency, and the Estimated Bubble Size

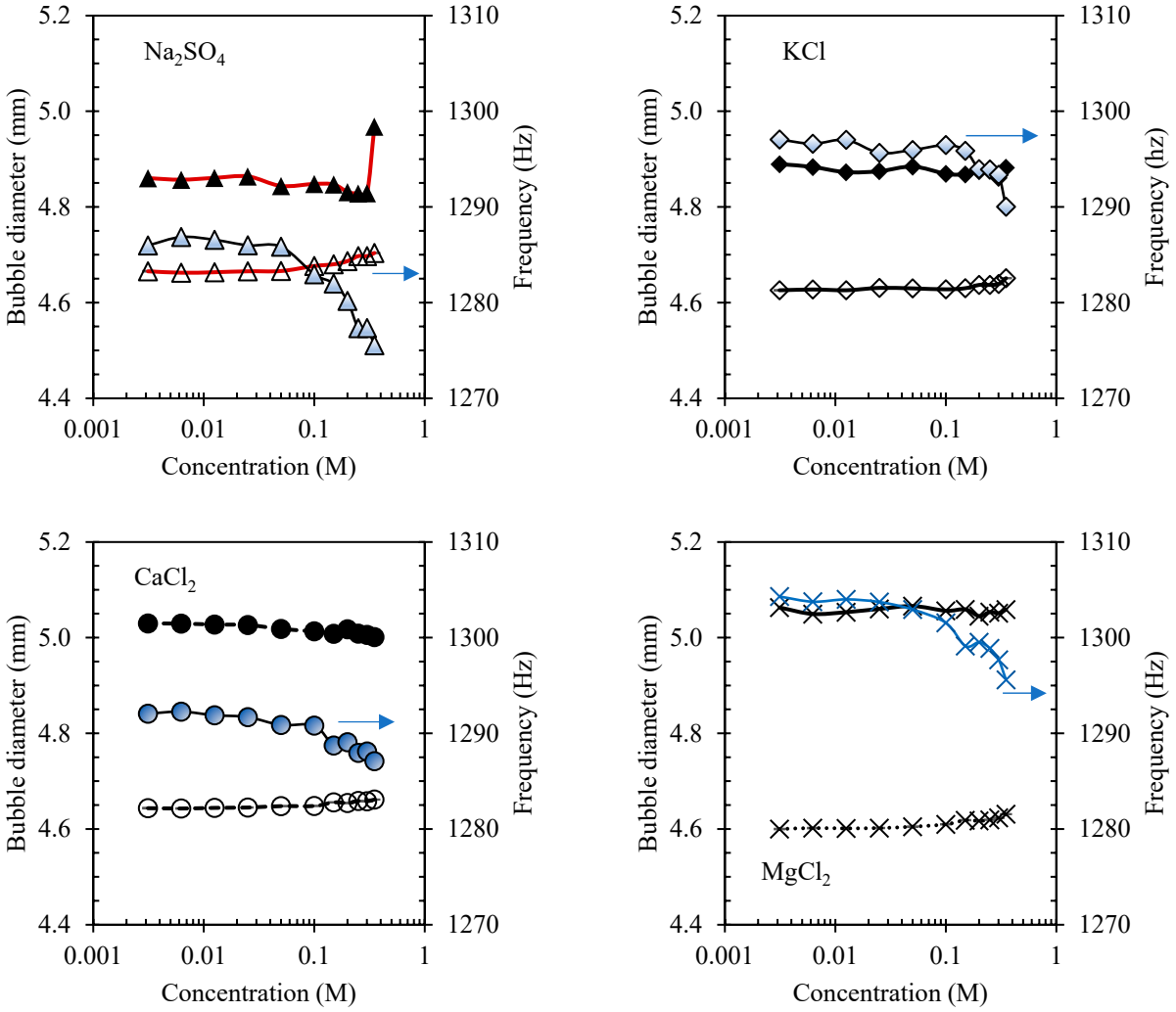


Figure A4. Acoustic frequency and bubble size in different salt solutions. The larger bubble size corresponds to those estimated from imaging.

References

1. Ball, P. Life of the ocean wave. *Nature* **2002**. [CrossRef]
2. Hofmeier, U.; Yaminsky, V.V.; Christenson, H.K. Observations of solute effects on bubble formation. *J. Colloid Interface Sci.* **1995**, *174*, 199–210. [CrossRef]
3. Prince, M.J.; Blanch, H.W. Bubble coalescence and break-up in air-sparged bubble columns. *AIChE J.* **1990**, *36*, 1485–1499. [CrossRef]
4. Chu, P.; Pax, R.; Li, R.; Langlois, R.; Finch, J.A. Using sound to study the effect of frothers on the breakaway of air bubbles at an underwater capillary. *Langmuir* **2017**, *33*, 3200–3207. [CrossRef] [PubMed]
5. Finch, J.A.; Nesset, J.E.; Acuña, C. Role of frother on bubble production and behaviour in flotation. *Miner. Eng.* **2008**, *21*, 949–957. [CrossRef]
6. Panjipour, R.; Karamoozian, M.; Albijanic, B. Bubble size distributions in gas–liquid–solid systems and their influence on flotation separation in a bubble column. *Chem. Eng. Res. Des.* **2021**, *167*, 96–106. [CrossRef]
7. Laskowski, J.S.; Cho, Y.S.; Ding, K. Effect of Frothers on Bubble Size and Foam Stability in Potash Ore Flotation Systems. *Can. J. Chem. Eng.* **2003**, *81*, 63–69. [CrossRef]
8. Kitchener, J.A.; Cooper, C.F. Current concepts in the theory of foaming. *Q. Rev. Chem. Soc.* **1959**, *13*, 71–97. [CrossRef]
9. Talanquer, V.; Oxtoby, D.W. Nucleation of bubbles in binary fluids. *J. Chem. Phys.* **1995**, *102*, 2156–2164. [CrossRef]
10. Blander, M.; Katz, J.L. Bubble nucleation in liquids. *AIChE J.* **1975**, *21*, 833–848. [CrossRef]
11. Cho, Y.S.; Laskowski, J.S. Bubble coalescence and its effect on dynamic foam stability. *Can. J. Chem. Eng.* **2002**, *80*, 299–305. [CrossRef]
12. Castro, S.; Miranda, C.; Toledo, P.; Laskowski, J.S. Effect of frothers on bubble coalescence and foaming in electrolyte solutions and seawater. *Int. J. Miner. Process.* **2013**, *124*, 8–14. [CrossRef]
13. Cho, Y.-S.; Laskowski, J.S. Effect of flotation frothers on bubble size and foam stability. *Int. J. Miner. Process.* **2002**, *64*, 69–80. [CrossRef]
14. Craig, V.S.J.; Ninham, B.W.; Pashley, R.M. Effect of electrolytes on bubble coalescence. *Nature* **1993**, *364*, 317–319. [CrossRef]
15. Firouzi, M.; Howes, T.; Nguyen, A.V. A quantitative review of the transition salt concentration for inhibiting bubble coalescence. *Adv. Colloid Interface Sci.* **2015**, *222*, 305–318. [CrossRef]
16. Weissenborn, P.K.; Pugh, R.J. Surface Tension of Aqueous Solutions of Electrolytes: Relationship with Ion Hydration, Oxygen Solubility, and Bubble Coalescence. *J. Colloid Interface Sci.* **1996**, *184*, 550–563. [CrossRef]
17. Craig, V.S.J. Bubble coalescence and specific-ion effects. *Curr. Opin. Colloid Interface Sci.* **2004**, *9*, 178–184. [CrossRef]
18. Kunz, W.; Nostro, P.L.; Ninham, B.W. The present state of affairs with Hofmeister effects. *Curr. Opin. Colloid Interface Sci.* **2004**, *9*, 1–18. [CrossRef]
19. Filippov, L.O.; Javor, Z.; Piriou, P.; Filippova, I.V. Salt effect on gas dispersion in flotation column–Bubble size as a function of turbulent intensity. *Miner. Eng.* **2018**, *127*, 6–14. [CrossRef]
20. Chu, P.; Waters, K.E.; Finch, J.A. Break-up in formation of small bubbles: Comparison between low and high frother concentrations. *Miner. Eng.* **2016**, *96*, 15–19. [CrossRef]
21. Chu, P.; Waters, K.E.; Finch, J.A. Break-up in formation of small bubbles: Break-up in a confined volume. *Colloids Surf. A Physicochem. Eng. Asp.* **2016**, *503*, 88–93. [CrossRef]
22. Chu, P.; Waters, K.E.; Finch, J.A. Break-up in formation of small bubbles: An energy consideration. *Can. Metall. Q.* **2017**, *56*, 30–34. [CrossRef]
23. Hinze, J.O. Fundamentals of the hydrodynamic mechanism of splitting in dispersion processes. *AIChE J.* **1955**, *1*, 289–295. [CrossRef]
24. Chu, P.; Finch, J.; Bournival, G.; Ata, S.; Hamlett, C.; Pugh, R.J. A review of bubble break-up. *Adv. Colloid Interface Sci.* **2019**, *270*, 108–122. [CrossRef]
25. Liao, Y.; Lucas, D. A literature review of theoretical models for drop and bubble breakup in turbulent dispersions. *Chem. Eng. Sci.* **2009**, *64*, 3389–3406. [CrossRef]
26. Hancer, M.; Celik, M.S.; Miller, J.D. The Significance of Interfacial Water Structure in Soluble Salt Flotation Systems. *J. Colloid Interface Sci.* **2001**, *235*, 150–161. [CrossRef] [PubMed]
27. Chen, M.; Lu, X.; Liu, X.; Hou, Q.; Zhu, Y.; Zhou, H. Specific counterion effects on the atomistic structure and Capillary-waves fluctuation of the water/vapor interface covered by sodium dodecyl sulfate. *J. Phys. Chem. C* **2014**, *118*, 19205–19213. [CrossRef]
28. Leighton, T. *The Acoustic Bubble*; Academic Press: Cambridge, MA, USA, 2012.
29. Minnaert, M., XVI. On musical air-bubbles and the sounds of running water. *Lond. Edinb. Dublin Philos. Mag. J. Sci.* **1933**, *16*, 235–248. [CrossRef]
30. Géradin, M.; Rixen, D.J. *Mechanical Vibrations: Theory and Application to Structural Dynamics*; John Wiley & Sons: Hoboken, NJ, USA, 2014.
31. Den Hartog, J.P. *Mechanical Vibrations*; Courier Corporation: Chelmsford, MA, USA, 1985.
32. Devin, C., Jr. Survey of thermal, radiation, and viscous damping of pulsating air bubbles in water. *J. Acoust. Soc. Am.* **1959**, *31*, 1654–1667. [CrossRef]
33. Tan, S.N.; Pugh, R.J.; Fornasiero, D.; Sedev, R.; Ralston, J. Foaming of polypropylene glycols and glycol/MIBC mixtures. *Miner. Eng.* **2005**, *18*, 179–188. [CrossRef]

34. Lucassen, J. Effect of surface-active material on the damping of gravity waves: A reappraisal. *J. Colloid Interface Sci.* **1982**, *85*, 52–58. [CrossRef]
35. Lemaire, C.; Langevin, D. Longitudinal surface waves at liquid interfaces: Measurement of monolayer viscoelasticity. *Colloids Surf.* **1992**, *65*, 101–112. [CrossRef]
36. Hühnerfuss, H.; Lange, P.A.; Walter, W. Relaxation effects in monolayers and their contribution to water wave damping: I. Wave-induced phase shifts. *J. Colloid Interface Sci.* **1985**, *108*, 430–441. [CrossRef]
37. Miller, C.A.; Neogi, P. *Interfacial Phenomena: Equilibrium and Dynamic Effects 139*; CRC Press: Boca Raton, FL, USA, 2007.
38. Quinn, J.J.; Kracht, W.; Gomez, C.O.; Gagnon, C.; Finch, J.A. Comparing the effect of salts and frother (MIBC) on gas dispersion and froth properties. *Miner. Eng.* **2007**, *20*, 1296–1302. [CrossRef]
39. Marrucci, G.; Nicodemo, L. Coalescence of gas bubbles in aqueous solutions of inorganic electrolytes. *Chem. Eng. Sci.* **1967**, *22*, 1257–1265. [CrossRef]
40. Lessard, R.R.; Zieminski, S.A. Bubble coalescence and gas transfer in aqueous electrolytic solutions. *Ind. Eng. Chem. Fundam.* **1971**, *10*, 260–269. [CrossRef]
41. Kracht, W.; Finch, J.A. Bubble break-up and the role of frother and salt. *Int. J. Miner. Process.* **2009**, *92*, 153–161. [CrossRef]
42. Kracht, W.; Finch, J.A. Using sound to study bubble coalescence. *J. Colloid Interface Sci.* **2009**, *332*, 237–245. [CrossRef] [PubMed]
43. Maldonado, M.; Quinn, J.J.; Gomez, C.O.; Finch, J.A. An experimental study examining the relationship between bubble shape and rise velocity. *Chem. Eng. Sci.* **2013**, *98*, 7–11. [CrossRef]
44. Quinn, J.J.; Maldonado, M.; Gomez, C.O.; Finch, J.A. Experimental study on the shape–velocity relationship of an ellipsoidal bubble in inorganic salt solutions. *Miner. Eng.* **2014**, *55*, 5–10. [CrossRef]
45. Sovechles, J.M.; Waters, K.E. Effect of ionic strength on bubble coalescence in inorganic salt and seawater solutions. *AIChE J.* **2015**, *61*, 2489–2496. [CrossRef]
46. Del Castillo, L.A.; Ohnishi, S.; Horn, R.G. Inhibition of bubble coalescence: Effects of salt concentration and speed of approach. *J. Colloid Interface Sci.* **2011**, *356*, 316–324. [CrossRef] [PubMed]